Supplementary Information

Origin of Screen-printed Metal Contact Losses in Crystalline Silicon Solar Cells

Authors

Myeong Sang Jeong[1,5], Sang Hee Lee[1,5], Sungjin Choi[1], Kwan Hong Min[1], Jong Hoon Lee[2], Min Gu Kang[1], Kyung Taek Jeong[1], Sang Kyu Kwak[3], Hee-eun Song[1*], Tae Kyung Lee[1,4*], and Sungeun Park[1*]

Affiliations

[1]*Photovoltaics Research Department, Korea Institute of Energy Research (KIER), 152 Gajeong-ro, Yuseong-gu, Daejeon 34129, Republic of Korea*

[2]*Ulsan National Institute of Science and Technology (UNIST) Central Research Facilities (UCRF), UNIST, Ulsan 44919, Republic of Korea*

[3]*Department of Energy Engineering, School of Energy and Chemical Engineering, UNIST, Ulsan 44919, Republic of Korea*

[4]*School of Materials Science and Engineering, Gyeongsang National University (GNU), Jinju 52828, Republic of Korea*

[5]These authors contributed equally

***Corresponding authors**

E-mail: hsong@kier.re.kr; tklee8865@gnu.ac.kr; separk@kier.re.kr

Supplementary Note 1. Effect of P doping configuration on MIGS and DBS

We investigated the effects of various P doping configurations on the MIGS and DBS based on the calculation results presented in **Figs. 5d and e**. By using the model systems displayed in **Supplementary Fig. 14a**, we calculated the integrated numbers of MIGS and DBS for different surface types and P doping configurations. As shown in **Supplementary Fig. 14b**, the number of MIGS depends on P doping type (a similar trend is observed for DBS in **Supplementary Fig. 14c**). In particular, when P doping occurred near the Ag–Si interface, the lowest number of MIGS (which was smaller than that of the pristine system) was obtained for the (111) surface. Meanwhile, P doping can also increase the number of MIGS if it is performed far from the Ag–Si interface (P doping$_{\text{type III}}$). Nevertheless, this P doping type had the most thermodynamically unfavorable formation energy (**Supplementary Fig. 14d**). Although all P doping configurations obtained for the (100) surface produced lower numbers of MIGS than that of the pristine system, they still exceeded the values obtained for the (111) surface, except for P doping$_{\text{type III}}$ (**Supplementary Fig. 14b**). Moreover, the difference between the numbers of MIGS and DBS on the (111) surface was much larger than that on the (100) surface regardless of the P doping configuration (**Supplementary Figs. 14b and 14c**). This indicates that the recombination process induced by the Si dangling bonds in the (111) surface is significantly inhibited by the Ag contact due to its epitaxial growth. Therefore, in the present study, the observed decrease in $J_{0.\text{metal}}$ is mainly caused by the lower number of DBS on the (111) surface containing the epitaxially grown Ag layer.

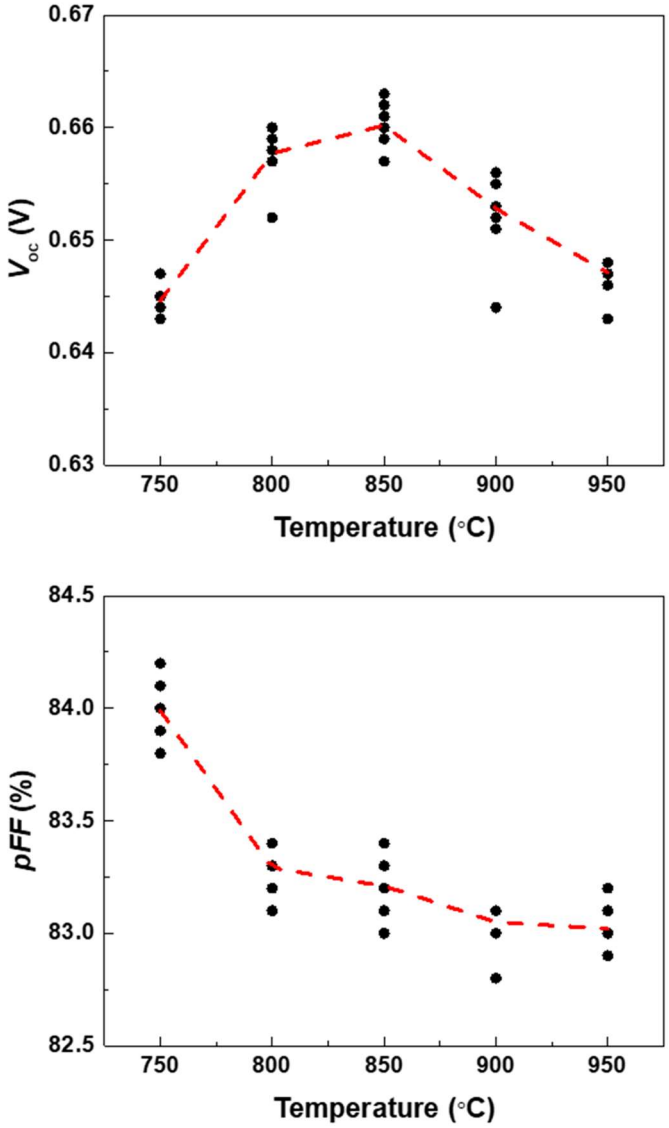

Supplementary Fig. 1 Parameters of the c-Si solar cell (V_{oc} and *pFF*) obtained at various firing temperatures. The red dashed lines indicate the average V_{oc} and *pFF* values.

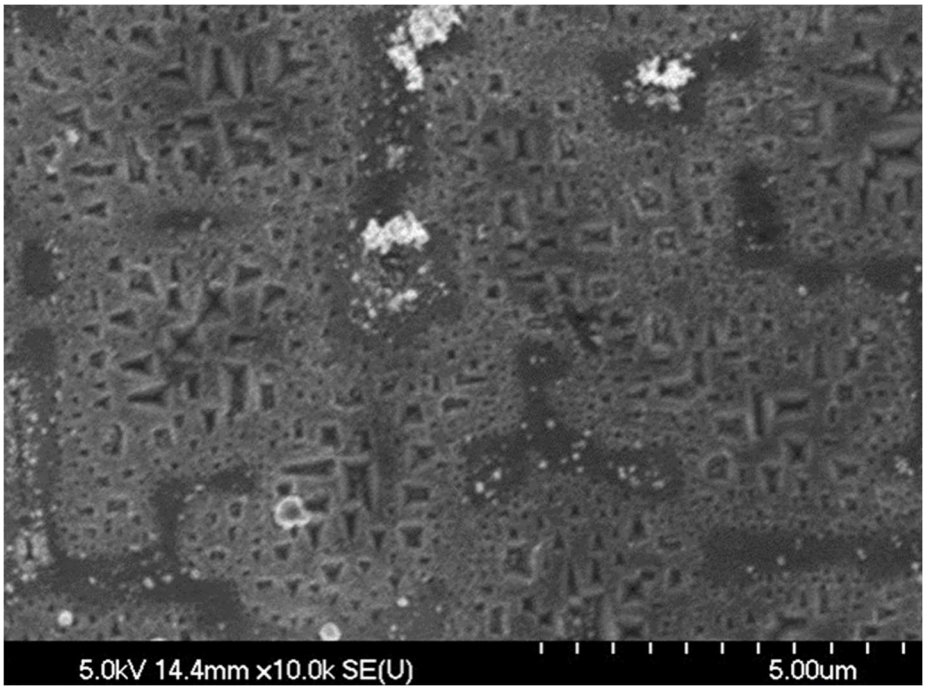

Supplementary Fig. 2 Morphology of the Si surface in the glass frit/SiN_x/Si structure after the firing process (T = 850 °C) determined by SEM. The glass frit was deposited by the screen printing method, and its etching was performed using a 10 wt.% HF solution (3 min).

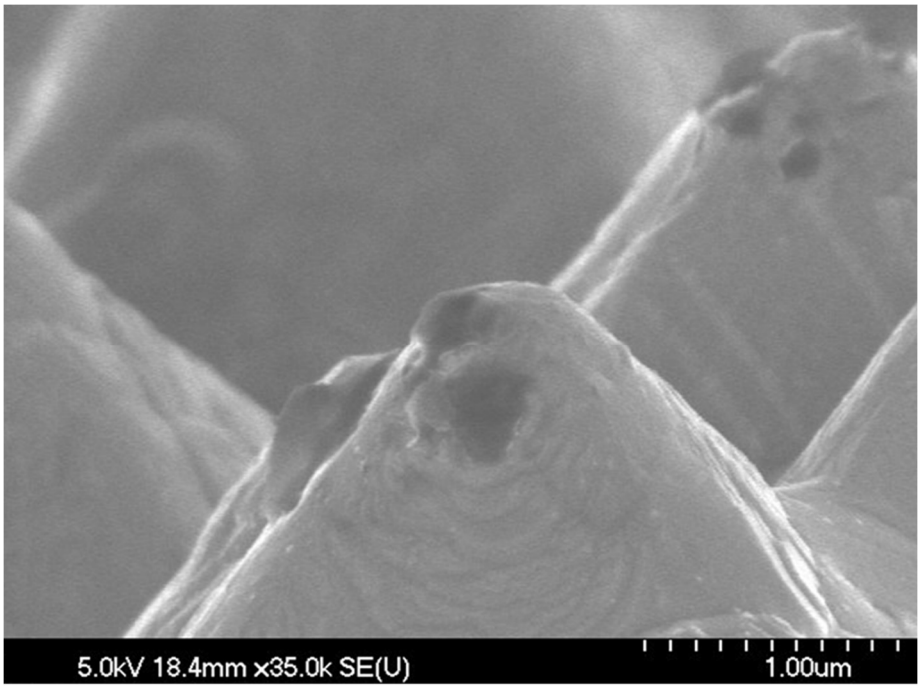

Supplementary Fig. 3 Morphology of the Ag-evaporated Si surface in the Ag/SiN_x/Si structure obtained after the firing process (T = 850 °C) by SEM.

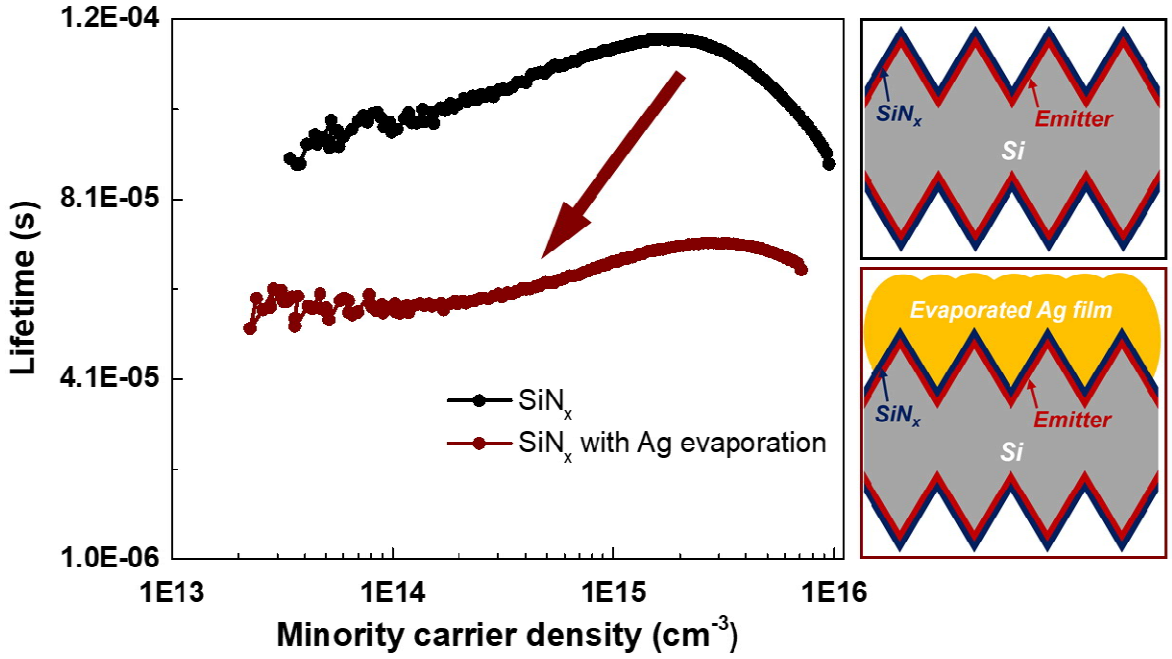

Supplementary Fig. 4 Lifetimes of the SiN_x/Si and Ag/SiN_x/Si structures obtained after the firing process (T = 850 °C). To determine the lifetime of the Ag/SiN_x/Si structure, the evaporated Ag film was removed using a 68 wt.% HNO_3 solution (3 min).

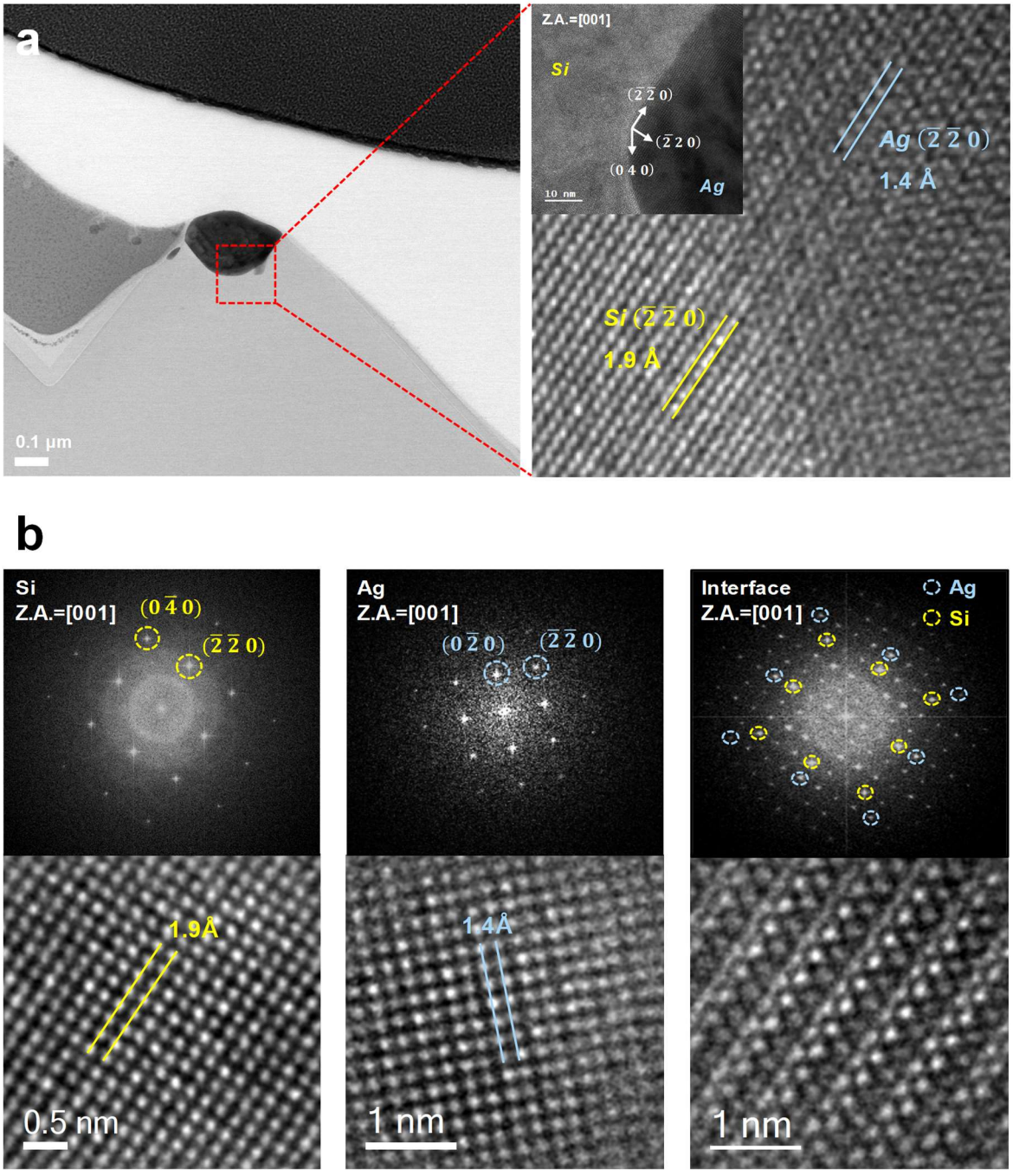

Supplementary Fig. 5 Analysis of the Ag–Si interfacial structure. a, HRTEM image (Z.A. = [001]). **b,** FFT pattern and filtered atom images of Si (left), Ag (middle), and the Ag–Si interface (right). The firing temperature is 850 °C.

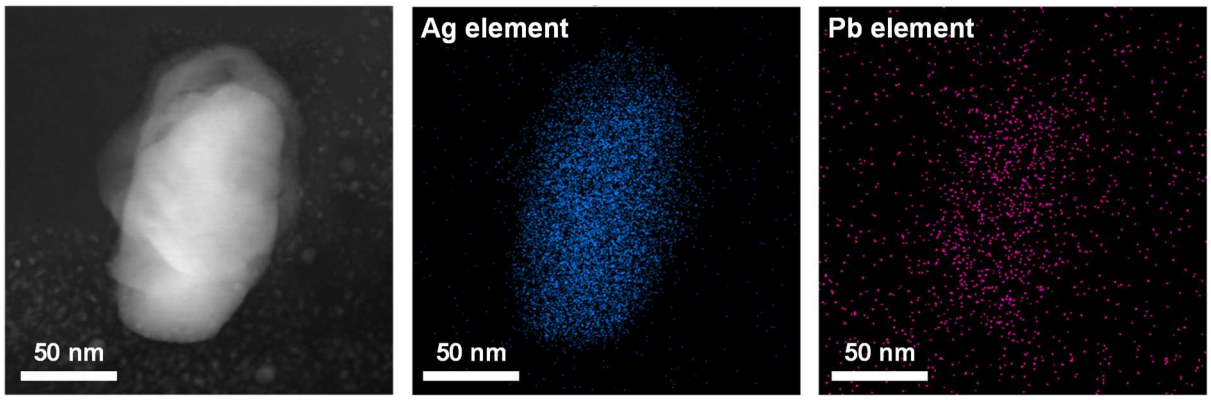

Supplementary Fig. 6 TEM–EDS mapping images of Ag and Pb elements (top view).

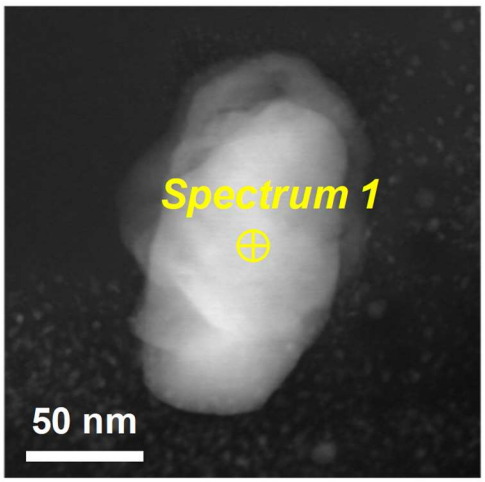

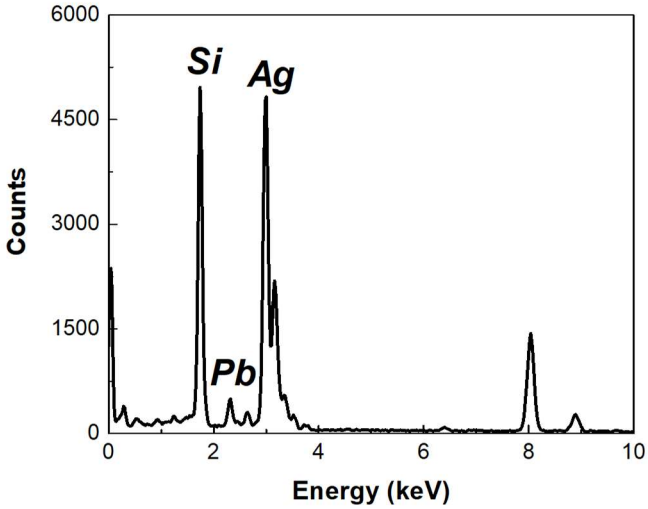

Element	Line type	k factor	Absorption correction	wt%	Atomic%
Ag	L series	1.823	1.00	97.54	98.70
Pb	M series	1.794	1.00	2.46	1.30
Total				100.00	100.00

Supplementary Fig. 7 TEM-EDS analysis of Pb atoms.

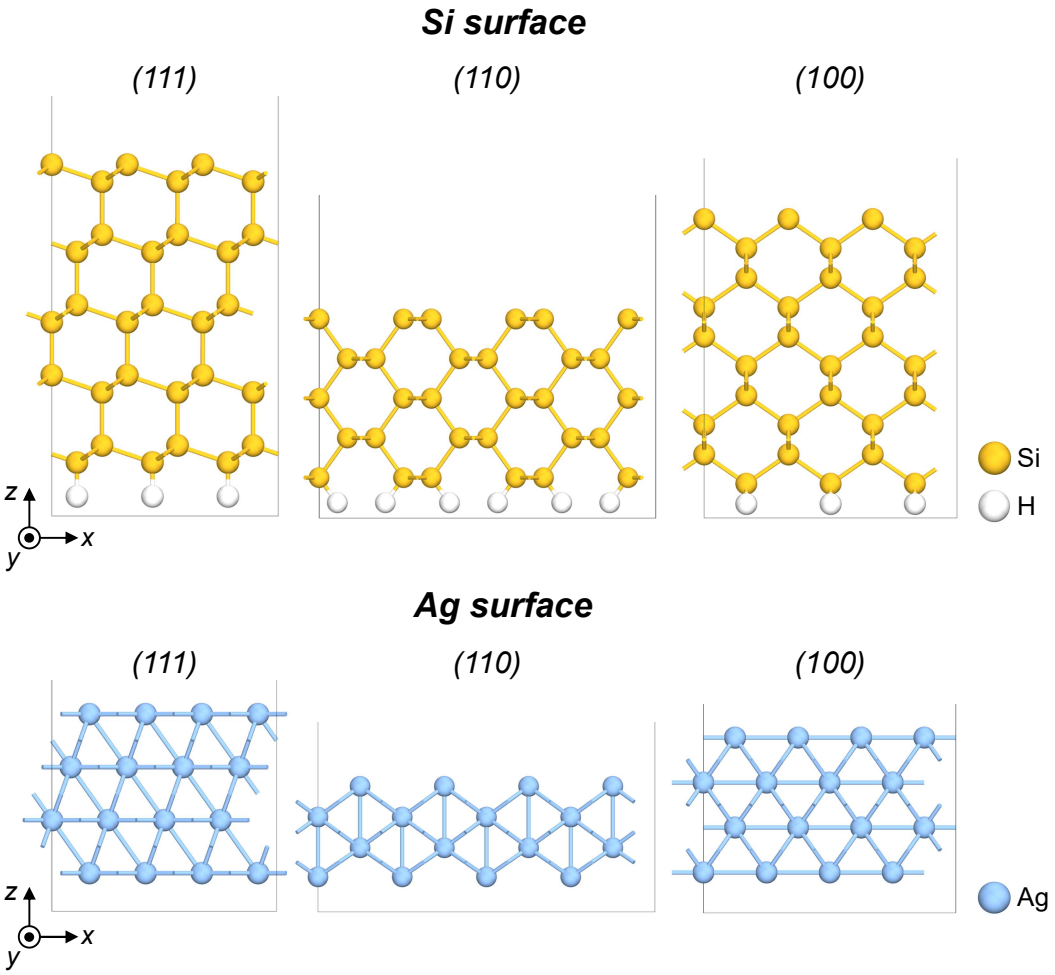

Supplementary Fig. 8 Model systems of the Si and Ag surfaces. Three different surface types ((111), (110), and (100)) were considered.

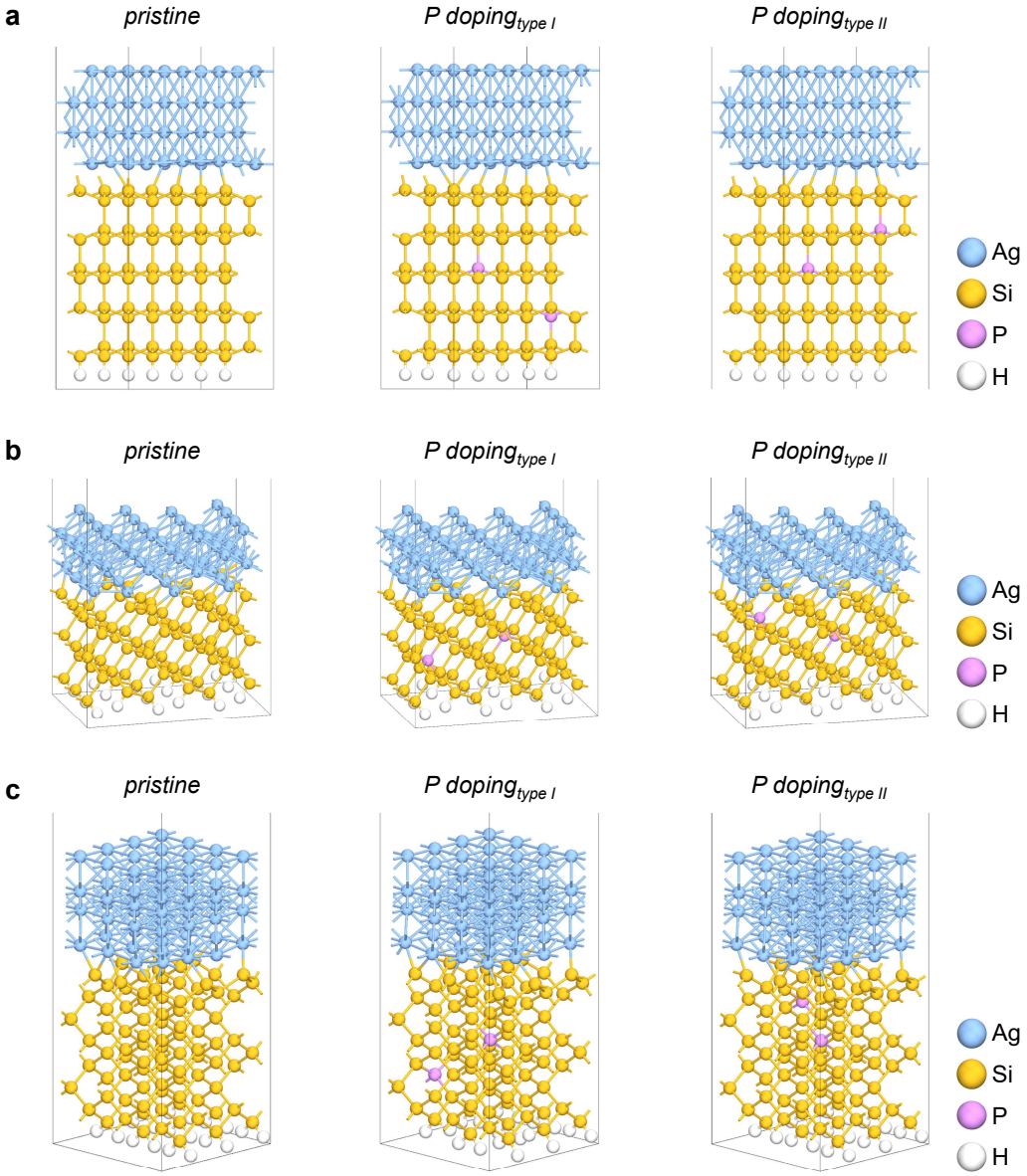

Supplementary Fig. 9 Model systems of the Ag–Si interfacial structures for various surface and P doping types. a-c, Three different types of Ag–Si interfaces (pristine, P doping$_{\text{type I}}$, and P doping$_{\text{type II}}$) obtained for the (111) (**a**), (110) (**b**), and (100) (**c**) surfaces. The numbers of Si and Ag atoms in the pristine systems are equal to 90 and 64, respectively, regardless of the surface type. In the P-doped systems, the number of P atoms is 2 regardless of surface type. The numbers of H atoms in the (111), (110), and (100) surface systems are equal to 9, 18, and 18, respectively. The H atoms and the bottom and top two layers of the Si and Ag surfaces are constrained by *x*- and *y*-axes, respectively.

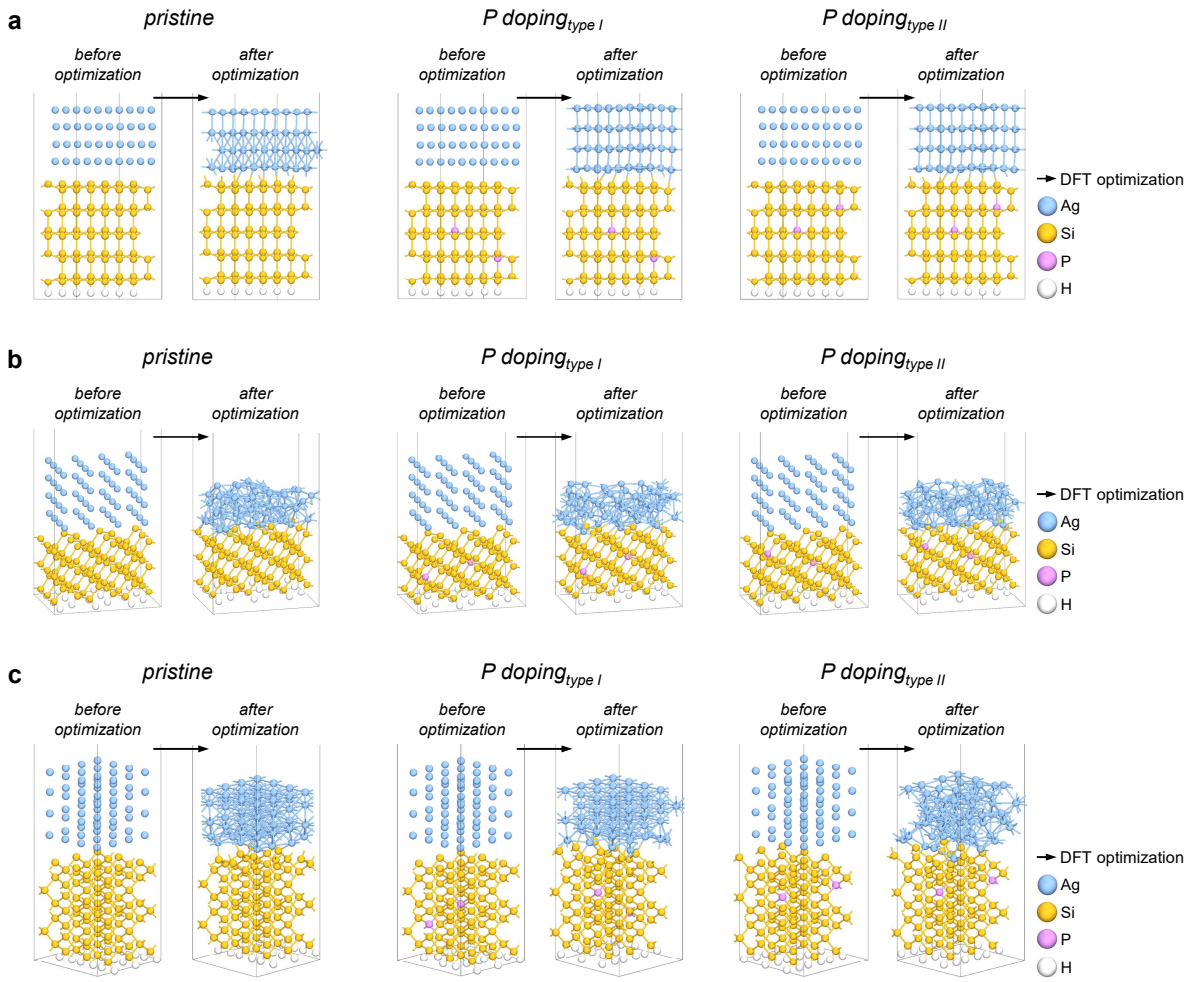

Supplementary Fig. 10 Model systems constructed for the non-epitaxial Ag–Si interfacial structures. a-c, Three Ag–Si interfacial structures (pristine, P doping$_{\text{type I}}$, and P doping$_{\text{type II}}$) obtained for the (111) (**a**), (110) (**b**), and (100) (**c**) surfaces. The numbers of Si and Ag atoms in the pristine systems are equal to 90 and 64, respectively, regardless of the surface type. In the P-doped systems, the number of P atoms is 2 regardless of the surface type. The numbers of H atoms in the (111), (110), and (100) surface systems are equal to 9, 18, and 18, respectively. The H atoms and the bottom two layers of Si surface are constrained by the *x*- and *y*-axes, respectively.

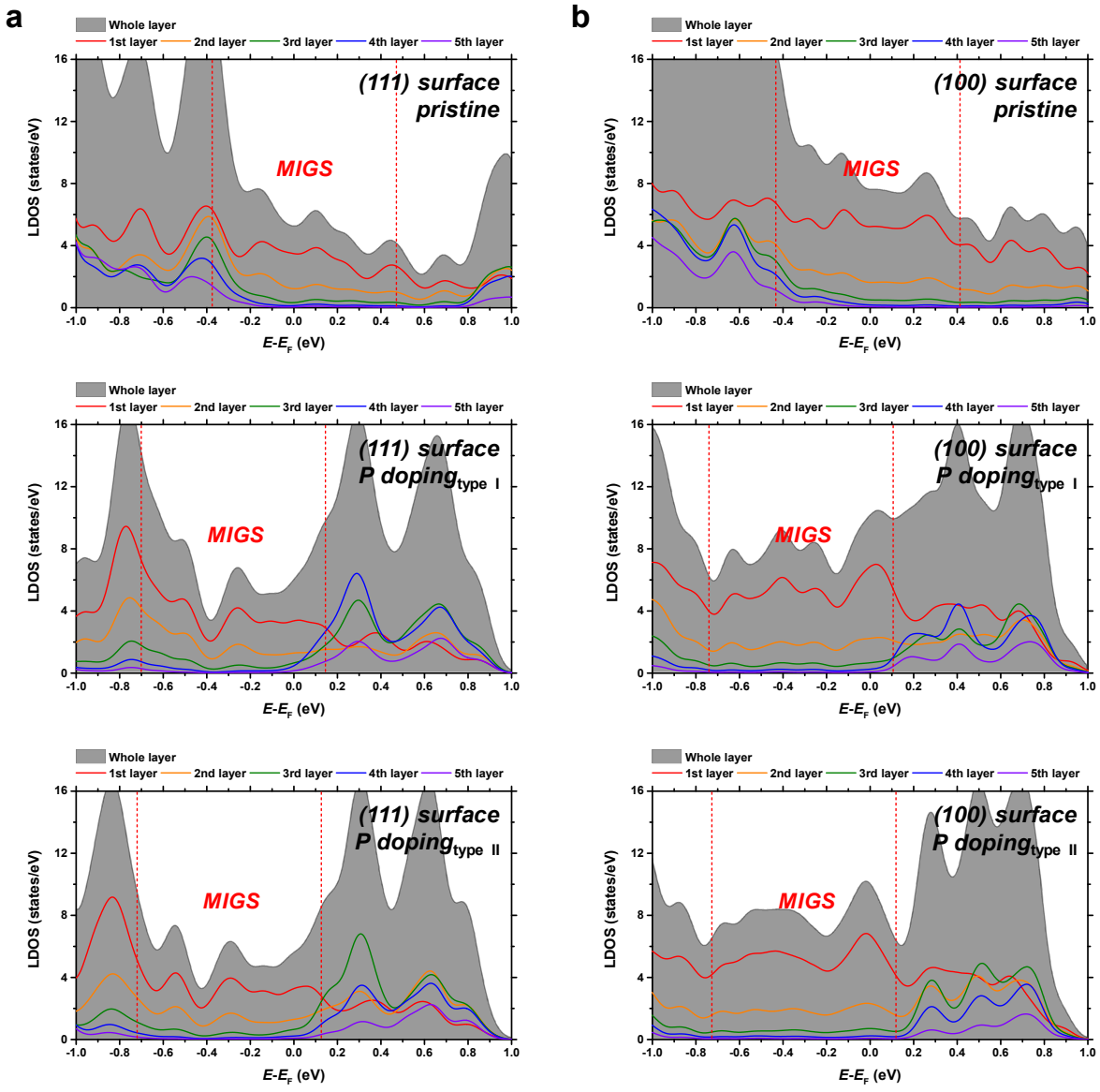

86

87 **Supplementary Fig. 11 LDOS calculated for the Si layers in the Ag–Si interfacial**

88 **structures. a,b,** LDOS of the three types of Ag–Si interfacial structures obtained for the (111)

89 (**a**) and (100) (**b**) surfaces. The red dashed lines indicate the MIGS regions.

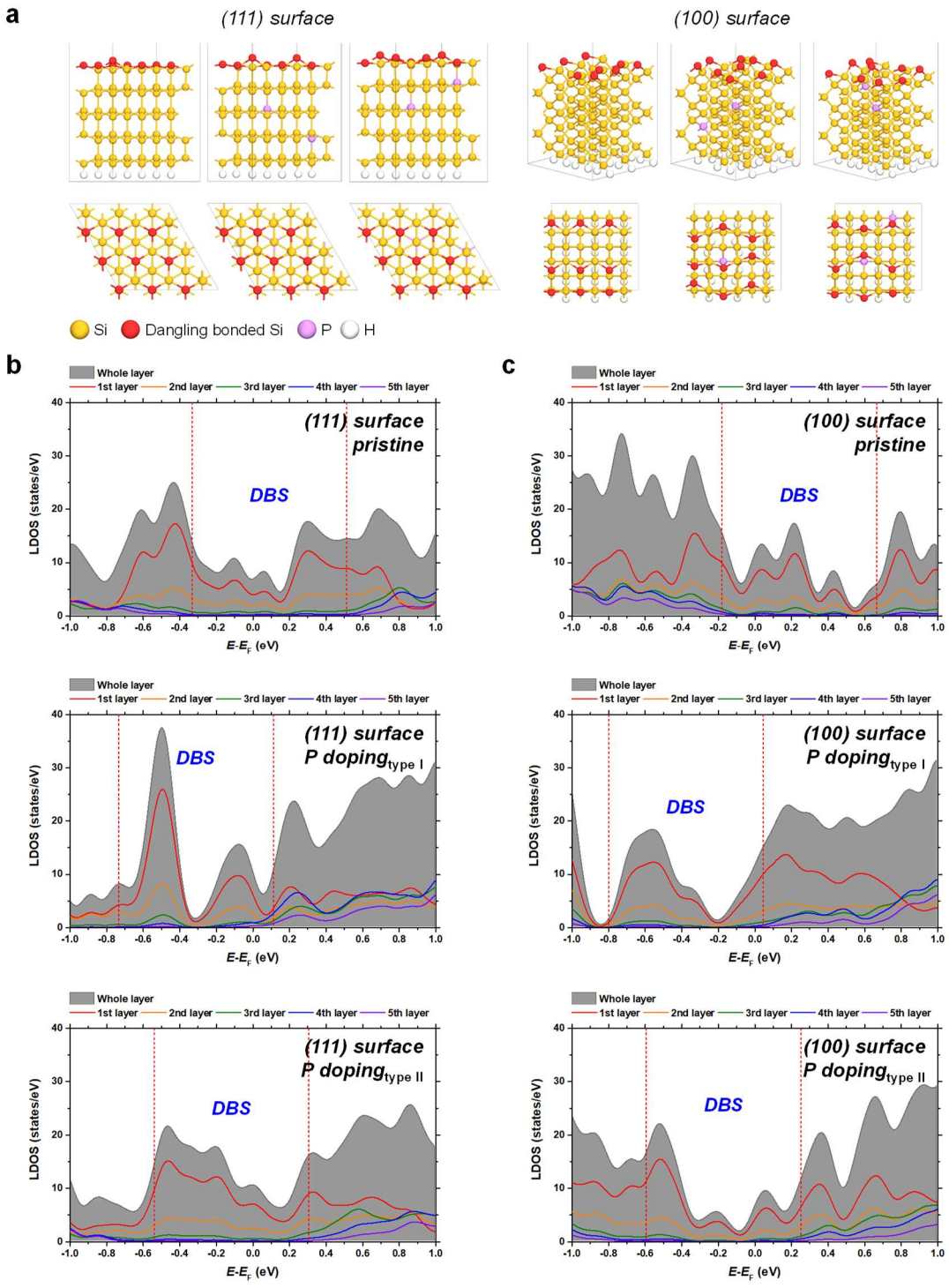

Supplementary Fig. 12 LDOS of the Si layers containing dangling bonds. a, Model systems of the (111) and (100) surfaces with dangling bonds. **b,c,** LDOS of the three types of Ag–Si interfacial structures obtained for the (111) (**b**) and (100) (**c**) surfaces. The red dashed lines indicate the DBS regions.

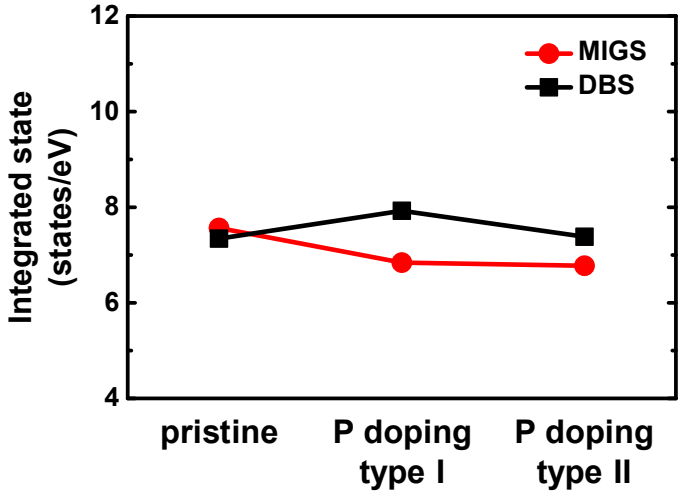

Supplementary Fig. 13 MIGS and DBS for Ag–Si interface$_{(100)\ surface}$ and Si$_{(100)\ surface}$ with dangling bonds, respectively.

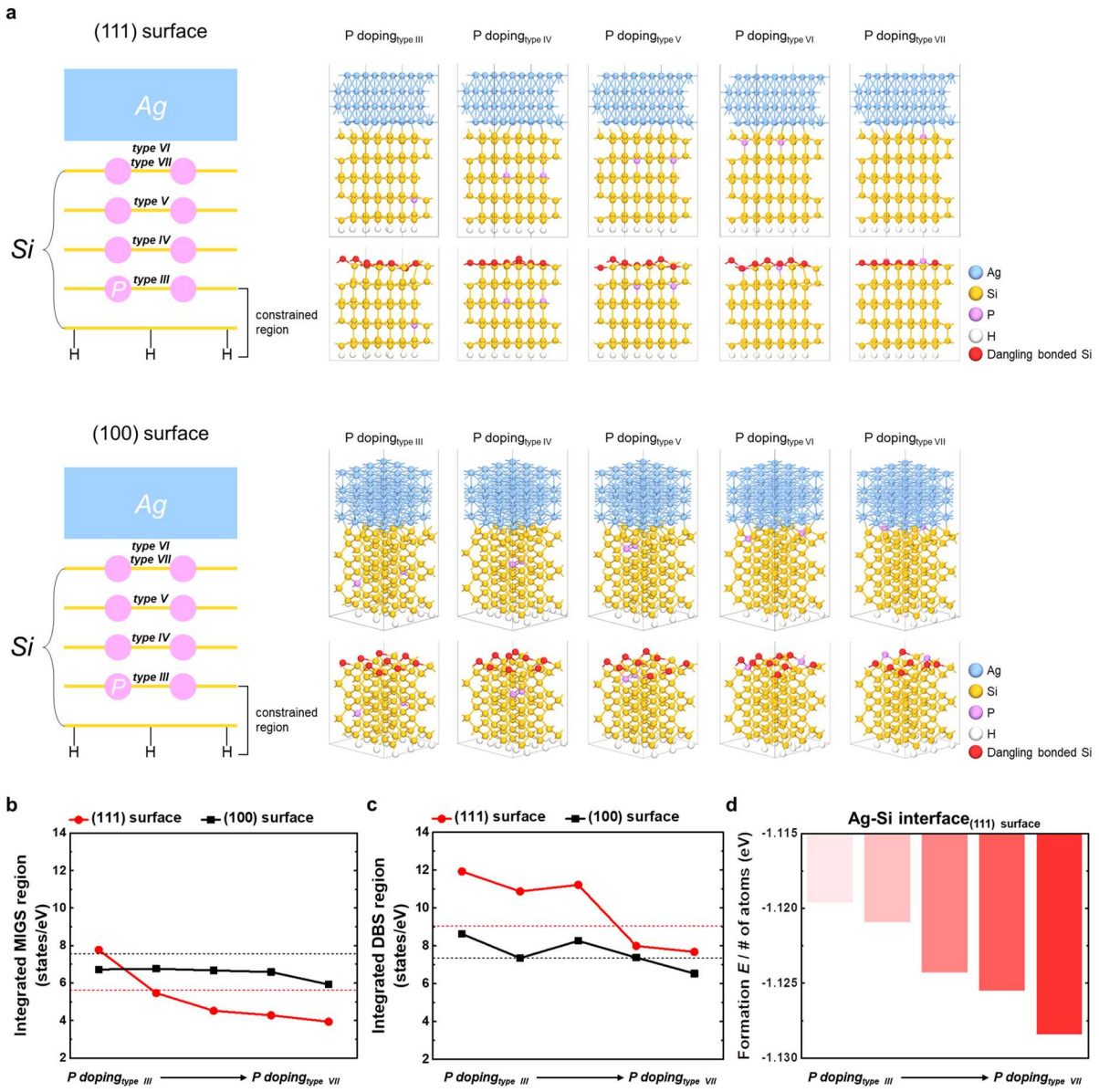

98

99 **Supplementary Fig. 14 Effects of P doping configuration on MIGS and DBS. a,** Model
100 systems of the five P doping configurations for the (111) and (100) surfaces of the Ag–Si
101 interface and Si surface structures containing dangling bonds. **b,c,** MIGS (**b**) and DBS (**c**) of
102 the Ag–Si interface and Si surface structure containing dangling bonds, respectively. The black
103 and red dashed lines indicate the MIGS and DBS of the pristine (non-doped) systems. **d,**
104 Formation energies of the Ag–Si interface$_{(111)\ surface}$ structure.